Journal of the Optical Society of America A
OPTICS, IMAGE SCIENCE, AND VISION

Propagation properties of right-hand circularly polarized Airy–Gaussian beams through slabs of right-handed materials and left-handed materials

JIAYAO HUANG,[1,2,†] ZIJIE LIANG,[1,2,†] FU DENG,[1,2] WEIHAO YU,[1,2] RUIHUANG ZHAO,[1,2] BO CHEN,[1,2] XIANGBO YANG,[1] AND DONGMEI DENG[1,2,*]

[1]Guangdong Provincial Key Laboratory of Nanophotonic Functional Materials and Devices, South China Normal University, Guangzhou 510631, China
[2]CAS Key Laboratory of Geospace Environment, University of Science & Technology of China, Chinese Academy of Sciences, Hefei 230026, China
*Corresponding author: dmdeng@263.net

Received 30 June 2015; revised 29 August 2015; accepted 4 September 2015; posted 23 September 2015 (Doc. ID 243422); published 19 October 2015

The propagation of right-hand circularly polarized Airy–Gaussian beams (RHCPAiGBs) through slabs of right-handed materials (RHMs) and left-handed materials (LHMs) is investigated analytically and numerically with the transfer matrix method. An approximate analytical expression for the RHCPAiGBs passing through a paraxial ABCD optical system is derived on the basis of the Huygens diffraction integral formula. The intensity and the phase distributions of the RHCPAiGBs through RHMs and LHMs are demonstrated. The influence of the parameter χ_0 on the propagation of RHCPAiGBs through RHM and LHM slabs is investigated. The RHCPAiGBs possess transverse-momentum currents, which shows that the physics underlying this intriguing accelerating effect is that of the combined contributions of the transverse spin and transverse orbital currents. Additionally, we go a step further to explore the radiation force including the gradient force and scattering force of the RHCPAiGBs.

OCIS codes: (010.3310) Laser beam transmission; (070.2590) ABCD transforms; (350.3618) Left-handed materials.

http://dx.doi.org/10.1364/JOSAA.32.002104

1. INTRODUCTION

In 1979, Berry and Balazs predicted that the fundamental Airy wave packet would be a solution of the Schrödinger equation in the context of quantum mechanics [1]. As one kind of nondiffracting beam, it is not only nondiffracting within a diffraction-free zone [2] and self-healing after passing through obstacles [3], but it also undergoes self-bending during propagation [2,4], which distinguishes the Airy beam from another nondiffracting beam such as the Bessel beam. As well, the Airy beam has been studied extensively due to its unique properties, especially its self-acceleration. However, infinite energy is carried in the Airy beam theoretically, signifying that the Airy beam with infinite energy is nonexistent in reality. In 2007, the finite energy Airy beam was first studied and was experimentally demonstrated in optics by Siviloglou and Christodoulides [4]. Airy–Gaussian (AiG) beams, a generalized form of the Airy beams, carry finite energy and maintain their approximate nondiffracting propagation properties within a finite distance of propagation [5]. The AiG beam propagates with a pattern between the Airy beam and the Gaussian beam, which is influenced by a parameter. AiG beams can be realized experimentally to a very good approximation [5].

Based on the current theoretical and experimental research, there are three properties during the propagation of the AiG beam: approximately nondiffracting, self-healing, and self-accelerating. Approximately nondiffracting means that it almost retains the shape of the intensity distributions during propagation. Self-healing means that the beam can be partially obstructed at one point, but will reform at a point further down the beam main lobe. Self-accelerating means the beam propagates along parabolic trajectories resulting from asymmetric transverse intensity patterns, similar to the ballistic trajectory under the effect of gravity.

Bandres and Gutiérrez-Vega [5] introduced the generalized AiG beam and analyzed propagation through optical systems described by ABCD matrices with complex elements. Deng and Li [6] have studied the propagation of the AiG beam in a strongly nonlocal medium analytically and numerically. Chen *et al.* [7] have shown the propagation of the AiG beam in a Kerr medium.

On the other hand, in 1968, Veselago first introduced the concept of left-handed materials (LHMs) with simultaneously negative permittivity and negative permeability [8]. However, due to the fact that such a LHM does not exist naturally, Veselago's research was not properly regarded over the last three decades. In the late 1990s, Pendry *et al.* put forward a model of a periodic array of metallic wires to obtain an effective negative permittivity [9,10], and an array of split-ring resonators to get an effective negative permeability [11]. The first artificial LHM was fabricated by Smith *et al.* [12].

Luo *et al.* [13] have studied the reversed propagation dynamics of Laguerre–Gaussian beams in left-handed materials. The propagation property of an $(1+1)$D Airy beam from right-handed material (RHM) to LHM has been investigated, and some useful numerical results were demonstrated by Lin and Pu [14]. Chen *et al.* [15] have investigated the $(2+1)$D Airy–Gaussian vortex (AiGV) beams propagating through slabs of RHMs and LHMs. Here, we investigate the $(2+1)$D right-hand circularly polarized Airy–Gaussian beams (RHCPAiGBs) propagating through slabs of RHMs and LHMs.

2. ANALYTICAL EXPRESSION OF THE RHCPAIGBS THROUGH AN OPTICAL ABCD SYSTEM

The initial plane is on the left side of the RHMs, and the z-axis is the propagation direction in the Cartesian coordinate system. Figure 1 shows that the LHMs slab in region 2 is surrounded by the common RHMs in region 1 and region 3. The beam propagates a distance of Z_1 in region 1, Z_2 in region 2, and Z_3 in region 3. When the RHCPAiGBs pass through the slab of LHMs, they will pass the interfaces $z = Z_1$ and $z = Z_1 + Z_2$ before they reach the plane $z = Z_1 + Z_2 + Z_3$ in the RHMs.

The optical field distribution of the RHCPAiGB at the initial plane in the Cartesian coordinate system can be written in the form [4,6]

$$\vec{E}(x_0, y_0, 0) = A_0 Ai\left(\frac{x_0}{w_1}\right) Ai\left(\frac{y_0}{w_2}\right) \exp\left(\frac{a x_0}{w_1} + \frac{a y_0}{w_2}\right) \times \exp\left(-\frac{x_0^2 + y_0^2}{w_0^2}\right)(\vec{e}_x - i\vec{e}_y), \quad (1)$$

where A_0 is the constant amplitude of the complex amplitude; $0 \le a < 1$ is the exponential truncation factor; w_0 is the beam waist size; w_1 and w_2, respectively, denote the arbitrary transverse scales in the x and y directions; $Ai(\cdot)$ is the Airy function [16]; and $\vec{e}_x$ and $\vec{e}_y$ denote the unit vectors along the x and y directions. We assume $w_1 = w_2 = \chi_0 w_0$, where χ_0 is the parameter controlling the beam to tend to a right-hand circularly polarized (RHCP) Airy beam with a smaller value, or a RHCP Gaussian beam with larger one. Figure 2 shows the intensity distribution of the RHCPAiGB at the input plane with parameters $A_0 = 1$, $w_1 = w_2 = 0.1$ mm, and $a = 0.1$. We can find the asymmetric transverse intensity of the RHCPAiGB, which results in the beam self-bending along the 45° axis.

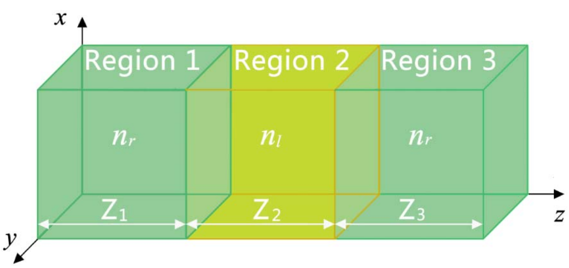

Fig. 1. Schematic diagram of the propagation system. The LHMs slab in region 2 is placed in between the RHMs in region 1 and region 3.

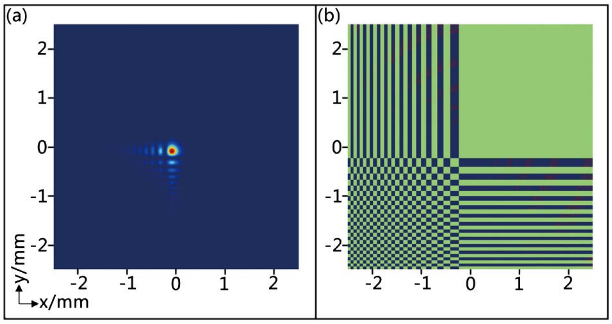

Fig. 2. (a) and (b) Intensity and phase distribution of the initial incident 2D RHCPAiGB at the input plane $z = 0$, respectively.

Now we discuss the propagation of the RHCPAiGBs through the slabs of RHMs and LHMs [17] under the paraxial approximation, and the ABCD matrix of the optical system can be written as [15]

$$\begin{pmatrix} A & B \\ C & D \end{pmatrix} = \begin{pmatrix} 1 & Z_2 \\ 0 & 1 \end{pmatrix}\begin{pmatrix} 1 & 0 \\ 0 & \frac{n_l}{n_r} \end{pmatrix}\begin{pmatrix} 1 & L \\ 0 & 1 \end{pmatrix} \times \begin{pmatrix} 1 & 0 \\ 0 & \frac{n_r}{n_l} \end{pmatrix}\begin{pmatrix} 1 & Z_1 \\ 0 & 1 \end{pmatrix} = \begin{pmatrix} 1 & Z_1 + L\frac{n_r}{n_l} + Z_2 \\ 0 & 1 \end{pmatrix}. \quad (2)$$

The paraxial propagation of the RHCPAiGBs through the optical ABCD system satisfies the Huygens diffraction integral [18],

$$\vec{E}(x, y, z) = \frac{ik}{2\pi B}\iint_{-\infty}^{\infty} \vec{E}(x_0, y_0, 0) \exp\left\{-\frac{ik}{2B}[A(x_0^2 + y_0^2) - 2(x_0 x + y_0 y) + D(x^2 + y^2)]\right\} dx_0 dy_0, \quad (3)$$

where $k = 2\pi/\lambda$ is the wavenumber in free space; λ is the wavelength of the incident light; A, B, and D are elements of the transfer matrix. Substituting Eq. (1) into Eq. (3), we obtain the ultimate output field distribution as

$$\vec{E}(x, y, z) = \frac{iA_0 k}{2BM} \exp(Q(x, y, z)) Ai(f(x)) Ai(g(y))(\vec{e}_x - i\vec{e}_y), \quad (4)$$

where

$$Q(x,y,z) = -\frac{ikD}{2B}(x^2+y^2) - \frac{k^2}{4B^2M}(x^2+y^2) + \frac{ik}{8BM^2}\left(\frac{x}{w_1^3}+\frac{y}{w_2^3}\right) + \frac{iak}{2BM}\left(\frac{x}{w_1}+\frac{y}{w_2}\right) + \frac{1}{96M^3}\left(\frac{1}{w_1^6}+\frac{1}{w_2^6}\right) + \frac{a}{8M^2}\left(\frac{1}{w_1^4}+\frac{1}{w_2^4}\right) + \frac{a^2}{4M}\left(\frac{1}{w_1^2}+\frac{1}{w_2^2}\right), \quad (5)$$

$$f(x) = \frac{ikx}{2BMw_1} + \frac{a}{2Mw_1^2} + \frac{1}{16M^2w_1^4}, \quad (6)$$

$$g(y) = \frac{iky}{2BMw_2} + \frac{a}{2Mw_2^2} + \frac{1}{16M^2w_2^4}, \quad (7)$$

with $M = \frac{1}{w_0^2} + \frac{ikA}{2B}$. In the next section, we can analyze the propagation of RHCPAiGBs through the paraxial optical system by employing Eq. (4) and the ABCD matrices with Eq. (2).

3. NUMERICAL RESULTS

To delve into the propagation properties of RHCPAiGBs through slabs of RHMs and LHMs, we carry out some numerical calculations and present the interesting findings. As discussed above, Eq. (4) is the general analytical expression of the field distribution of the RHCPAiGBs propagating through the optical ABCD system. We suppose that $A_0 = 1$, $a = 0.1$, $n_r = 1$, $n_l = -1$, $\lambda = 632.8$ nm, $\chi_0 = 0.05$, and $w_1 = w_2 = 0.1$ mm. The Rayleigh distance of the beam is $Z_R = kw_1^2/2 = 4.9646$ cm.

We suppose that there is no reflection at the interfaces $z = Z_1$ and $z = Z_1 + Z_2$.

Figures 3(a1)–3(a8) indicate the normalized intensity of the 1D RHCPAiGBs taken at different propagation distances marked by the dashed lines in Fig. 3(d). According to these figures, the translation of both the main lobe and minor lobes of the 1D RHCPAiGBs toward the positive x-axis occurred when propagating from $z = 0$ to $z = 12Z_R$ and from $z = 24Z_R$ to $z = 36Z_R$, and translation toward the negative x-axis occurred when propagating from $z = 12Z_R$ to $z = 24Z_R$ and from $z = 36Z_R$ to $z = 48Z_R$. Figures 3(b1)–3(b8) describe the corresponding transverse normalized intensity patterns. It can be clearly seen that the beam takes displacement along the 45° axis resulting from its distinctive symmetry (since $w_1 = w_2$). Figures 3(c1)–3(c8) depict the corresponding phase distribution. Considering that the acceleration of the RHCPAiGBs occurs along the 45° axis, we gain a numerically simulated side view of the RHCPAiGBs' propagation in the plane $y = x$, demonstrated in Fig. 3(d).

It is clearly seen that the RHCPAiGB experiences self-bending and goes along a parabolic trajectory when it passes through the slab of RHMs in region 1. When passing through the interface at $z = Z_1$, the beam undergoes refraction between the RHMs and LHMs. The refracted beam and the incident beam, however, are on one side of the interface normal.

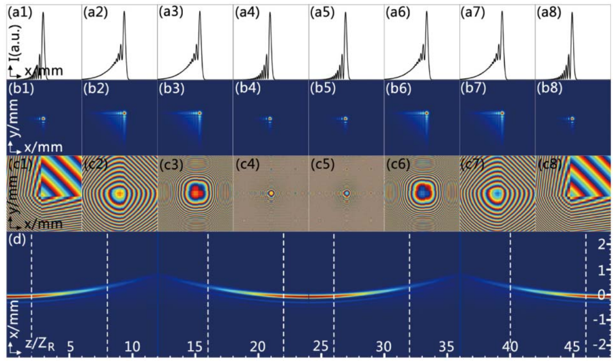

Fig. 3. Numerical demonstrations of the RHCPAiGBs propagating through slabs of RHMs and LHMs: (a1)—(a8) the intensity distributions of the 1D RHCPAiGBs at the positions $z = 2Z_R$, $8Z_R$, $16Z_R$, $22Z_R$, $26Z_R$, $32Z_R$, $40Z_R$, and $46Z_R$, marked by the dashed lines in (d); (b1)–(b8) the corresponding intensity distributions of the 2D RHCPAiGBs in (a); (c1)–(c8) the corresponding phase distributions at different positions; (d) numerically simulated side-view propagation of the RHCPAiGBs. The solid lines indicate the interfaces.

In fact, the beam obeys Snell's law at the interface because the refracted light inside the LHMs will make a negative angle with the interface normal. Afterward, the beam goes along a symmetric parabolic trajectory in LHMs. After the beam passes through the interface at $z = Z_1 + Z_2$, we can find that it experiences an inverse parabolic bending in region 3, namely, the LHMs slab acting as a perfect lens for the RHCPAiGB [19].

Interestingly, when comparing the Airy Gaussian vortex (AIGV) beam and RHCPAiGB beam, we can find that they transmit at the same trajectory when propagating through slabs of RHMs and LHMs. In spite of this, they have some different transmission characteristics. For instance, the maximum energy of the AIGV beam in the process of transmission symmetrically distributes far away from the center of the slabs while the maximum energy of the RHCPAiGBs distributes at the center. In addition, from the phase diagram, obviously, the AIGV beam possesses the vortex characteristic, but the RHCPAiGB does not [15].

Next, we make a comparison of the beam propagating different distances through slabs of RHMs and LHMs. As shown in Fig. 4, the RHCPAiGB is reconstructed after it passes through the slab of LHMs in region 2, and experiences an inverse process in region 3. At the distance $z = Z_1 + Z_2 + Z_3$, both the transverse intensity distribution and the phase of the RHCPAiGBs return to the original state ($z = 0$). Therefore, what can be expected is that the beam will maintain its intensity at a particular level to keep propagating like a zigzag wave regardless of passing through the arbitrary distances of alternating slabs of RHMs and LHMs, and that its intensity periodically repeats in every slab.

For observing the changes of intensity of the RHCPAiGBs with different χ_0, the peak intensity of the RHCPAiGBs is shown in Fig. 5. As χ_0 is increased, the peak intensity along the beam propagation changes more rapidly. In addition, the peak intensity of the RHCPAiGBs with larger χ_0 is more weakened than that with a smaller one at the same propagation distance.

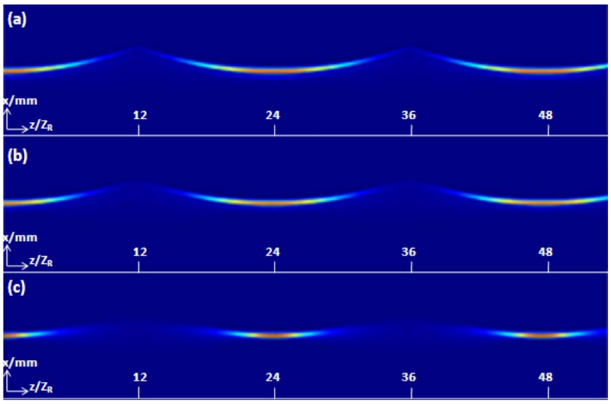

Fig. 4. Numerical demonstrations of the RHCPAiGBs propagating through RHM and LHM slabs: (a)–(c) Numerically simulated side-view propagation of the RHCPAiGBs with different distance slabs $Z_1 = 12$, $Z_2 = 24$, $Z_3 = 18$, respectively, with $\chi_0 = 0.05$ in (a), $\chi_0 = 0.1$ in (b), and $\chi_0 = 0.3$ in (c).

The time-averaged linear momentum density currents can be taken as the combined contributions of the spin and the orbital parts [20,21],

$$\vec{P}(\vec{r}) = \vec{P}_s(\vec{r}) + \vec{P}_o(\vec{r}), \tag{8}$$

where the orbital term is identified by the macroscopic energy current concerning an arbitrary reference point and is independent of the polarization. The spin term gets involved in the phase between orthogonal field components and is completely determined by the state of polarization [22]. In a monochromatic optical beam, the spin and orbital currents can be, respectively, expressed as [20,21]

$$\vec{P}_s(\vec{r}) = \mathrm{Im}[(\vec{E} \cdot \nabla)\vec{E}^*], \tag{9}$$

$$\vec{P}_o(\vec{r}) = \mathrm{Im}[\vec{E}^* \cdot (\nabla)\vec{E}], \tag{10}$$

where $\nabla = \frac{\partial}{\partial x}\vec{e}_x + \frac{\partial}{\partial y}\vec{e}_y + \frac{\partial}{\partial z}\vec{e}_z$ is the nabla symbol, $\vec{e}_z$ denotes the unit vector along the z direction, and $*$ denotes the complex conjugate.

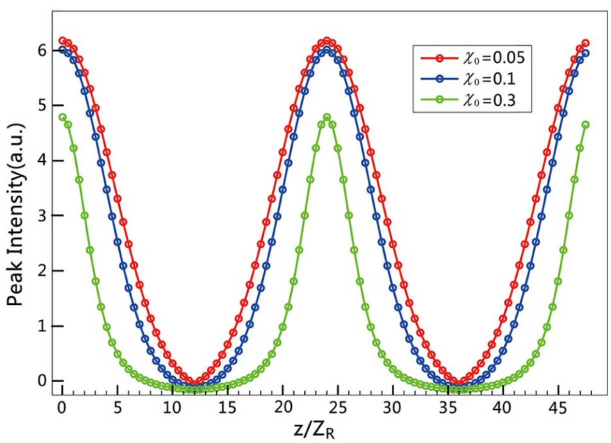

Fig. 5. Peak intensity distributions of the RHCPAiGBs with different χ_0.

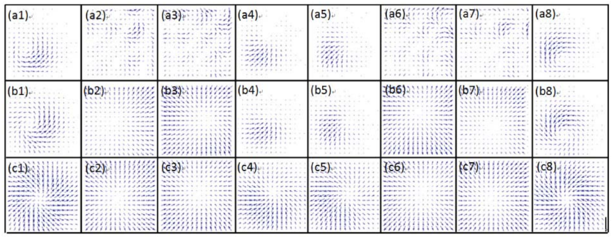

Fig. 6. Numerical demonstrations of the RHCPAiGBs propagating through slabs of RHMs and LHMs: (a1)–(a8) show the spin current of the RHCPAiGBs at the positions marked by the dashed lines in Fig. 3(d) with $\chi_0 = 0.05$; all are the same as those in (a1)–(a8) except $\chi_0 = 0.3$ in (b1)–(b8) and $\chi_0 = 1$ in (c1)–(c8).

We perform numerical simulations of the spin current and the orbital current of the RHCPAiGBs with $\chi_0 = 0.05, 0.3, 1$, respectively. Figures 6 and 7 show that the smaller χ_0 is, the stronger the aggregation of the spin current and the orbital current of the RHCPAiGBs is. As we know, the spin current and the orbital current are the global reaction of accelerating characteristics for the RHCPAiGBs. In other words, χ_0 with a small value is conducive to the self-accelerating of the RHCPAiGBs, nevertheless, the property of focused energy is lost. In addition, we find a funny phenomenon that whatever the parameter χ_0 holds, the variation trend of the spin current and the orbital current is almost identical.

Last, we explore the radiation forces of the RHCPAiGBs. The gradient force and the scattering force are deemed to be two kinds of radiation force. The gradient force is caused by the inhomogeneous distribution of the energy density and has the same direction as that of the optical intensity gradient. We assume that a microparticle with refractive index n_1 is struck by the beam. By employing the vector identity and the solution of the Maxwell equations, the gradient force can be written as [23]

$$\vec{F}_{\mathrm{grad}}(x, y, z, t) = [\vec{p}(x, y, z, t) \cdot \nabla]\vec{E}(x, y, z, t), \tag{11}$$

where $\vec{p}(x, y, z, t) = 4\pi n_2^2 \varepsilon_0 r_0^3 \left(\frac{m^2-1}{m^2+2}\right)\vec{E}(x, y, z, t)$ is the electric dipole moment of the particle [24,25], $m = \frac{n_1}{n_2}$ is the relative refractive index of the particle, n_2 is the refractive index of the surrounding medium, r_0 is the radius of the microparticle, and ε_0 is the permittivity of vacuum. When the particle is in steady state, its gradient force is the time average [23],

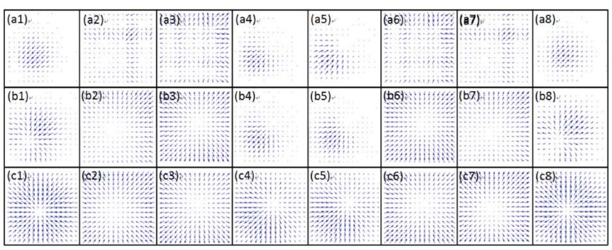

Fig. 7. Numerical demonstrations of the RHCPAiGBs propagating through slabs of RHMs and LHMs: (a1)–(a8) show the orbital current of the RHCPAiGBs at the positions marked by the dashed lines in Fig. 3(d) with $\chi_0 = 0.05$; all are the same as those in (a1)–(a8) except $\chi_0 = 0.3$ in (b1)–(b8) and $\chi_0 = 1$ in (c1)–(c8).

$$\vec{F}_{\mathrm{grad}}(x,y,z) = \frac{2\pi n_2 r_0^3}{c}\left(\frac{m^2-1}{m^2+2}\right)\nabla I(x,y,z), \qquad \textbf{(12)}$$

where c is the light velocity, $I(x,y,z) = cn_2\varepsilon_0 \frac{|E(x,y,z)|^2}{2}$.

The scattering force is associated with the scattering of light caused by the change of the electromagnetic momentum. It is in the same direction as the propagation of the beam. The scattering force can be expressed as [23]

$$\vec{F}_{\mathrm{scat}}(x,y,z) = \frac{n_2}{c} C_{\mathrm{pr}_0} I(x,y,z)\vec{e}_z, \qquad \textbf{(13)}$$

where C_{pr_0} is the radiation pressure section of the particle. Taking the isotropy of the particle into consideration, the radiation pressure section of the particle is equal to the scattering force section of the scatterer:

$$C_{\mathrm{pr}_0} = C_{\mathrm{scat}} = \frac{8}{3}\pi(ka)^4 r_0^2\left(\frac{m^2-1}{m^2+2}\right)^2. \qquad \textbf{(14)}$$

As you can see in Eq. (13), the positive or negative scattering force is determined by the sign of the refractive index n_2 of the surrounding medium. For scattering force in LHMs, parameter n_2 is negative, which means that the scattering force is also negative. Therefore, what can be explained is that a negative force can be observed in LHMs.

From Eq. (12) and Eq. (13), on the one hand, we can see that the gradient force of particles with high relative refractive index aims at the place with the maximum value of the intensity gradient, pulling the particles toward the maximum points. On the other hand, the scattering force aims at the direction of the beam's propagation, driving the particles to move along the optical axis when passing through the RHMs slabs in region 1 and region 3; diametrically, it aims against the direction of the beam's propagation, driving the particles to move against the optical axis when propagating through the LHMs slab in region 2. When the gradient force is stronger than the scattering force, the particle will be trapped at the maximum points of the intensity gradient in the interface $z = 12Z_R$. Owing to the RHCPAiGBs accompanied by a series of minor lobes, the particles will not only be trapped in the main lobe, but also in the minor lobes, so then more traps will be generated along the propagation of the RHCPAiGBs.

Figure 8 indicates the section distributions of the transverse gradient force of the RHCPAiGBs for the particles with

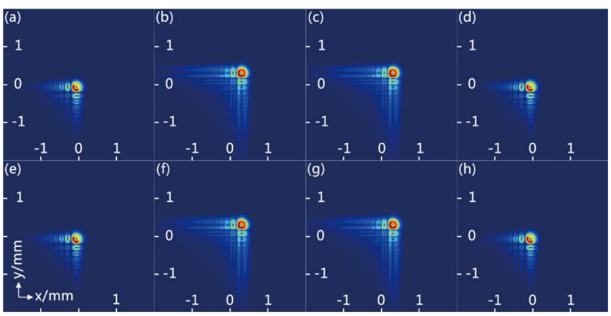

Fig. 8. Section distributions of the transverse gradient force of the RHCPAiGBs for the particles with $n_1 = 1.50$, $r_0 = 60$ nm: (a)–(h) the distribution at the distances marked by the dashed lines in Fig. 3(d), respectively.

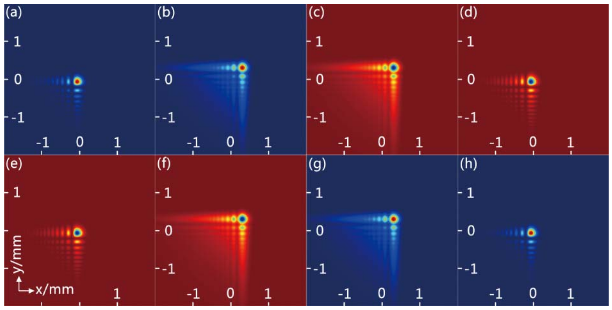

Fig. 9. Section distributions of the scattering force of the AiG beam along the z direction for the particles. All parameters are the same as those in Fig. 8.

$n_1 = 1.50$, $r_0 = 60$ nm. It can be seen that those particles struck by the beam are driven by the gradient force. According to Eq. (12) and Fig. 8, the forces aim toward the maximum value of the intensity gradient, namely, the centers of the main lobe and minor lobes. Around the centers of the main lobe and minor lobes, the gradient forces are stronger; nevertheless, they are vanishing at the centers. Figure 9 shows the section distributions of the scattering force of the RHCPAiGBs along the z direction for the particles with $n_1 = 1.50$, $r_0 = 60$ nm. According to Eq. (13) and Fig. 9, it is not hard to see that those particles struck by the beam in RHMs will be driven by the scattering force aiming in the direction of the beam's propagation. Meanwhile, the closer to the centers of the lobes the particles are, the stronger the scattering forces are. However, those particles struck by the beam in LHMs will be driven against the scattering forces aiming in the direction of the beam's propagation; similarly, the forces are stronger at the centers of the lobes.

4. CONCLUSIONS

In conclusion, we investigate the properties of the RHCPAiGBs through RHMs and LHMs. It is shown that the RHCPAiGB goes along a parabolic trajectory when it passes through the LHMs as well as through the RHMs. After it propagates through the slab of LHMs in region 2, the intensity and the phase distribution of the RHCPAiGB will return to their original states in the slab of RHMs in region 3. We also investigate the influence of the parameter χ_0 on the propagation of the RHCPAiGB. The physics underlying this intriguing accelerating effect of the RHCPAiGBs is the combined contributions of the transverse spin and the transverse orbital currents. In addition, χ_0 with a larger value results in the peak intensity of the beam changing more rapidly so that the energy of the beam will be focused seemingly. Last, the radiation forces of the RHCPAiGBs have been discussed. When the gradient force is stronger than the scattering force, the particle will be trapped at the maximum points of the intensity gradient in the interface $z = 12Z_R$. Owing to the RHCPAiGBs accompanied by a series of minor lobes, more traps will be generated along the propagation of the RHCPAiGBs.

†These authors contributed equally to this work.

Funding. Chinese Academy of Sciences (CAS) Key Laboratory of Geospace Environment, University of Science and Technology of China; Foundation of Cultivating Outstanding Young Scholars (Thousand, Hundred, Ten Program) of Guangdong Province in China; National Natural Science Foundation of China (NSFC) (11374107, 11374108, 10904041); National Training Program of Innovation and Entrepreneurship for Undergraduates (2015093).

REFERENCES

1. M. V. Berry and N. L. Balazs, "Nonspreading wave packets," Am. J. Phys. **47**, 264–267 (1979).
2. G. A. Siviloglou, J. Broky, A. Dogariu, and D. N. Christodoulides, "Observation of accelerating Airy beams," Phys. Rev. Lett. **99**, 213901 (2007).
3. J. Broky, G. A. Siviloglou, A. Dogariu, and D. N. Christodoulides, "Self-healing properties of optical Airy beams," Opt. Express **16**, 12880–12891 (2008).
4. G. A. Siviloglou and D. N. Christodoulides, "Accelerating finite energy Airy beams," Opt. Lett. **32**, 979–981 (2007).
5. M. A. Bandres and J. C. Gutiérrez-Vega, "Airy-Gauss beams and their transformation by paraxial optical systems," Opt. Express **15**, 16719–16728 (2007).
6. D. Deng and H. Li, "Propagation properties of Airy-Gaussian beams," Appl. Phys. B **106**, 677–681 (2012).
7. C. D. Chen, B. Chen, X. Peng, and D. M. Deng, "Propagation of Airy-Gaussian beam in Kerr medium," J. Opt. **17**, 035504 (2015).
8. V. G. Veselago, "The electrodynamics of substances with simultaneously negative value of ε and μ," Sov. Phys. Usp. **10**, 509–514 (1968).
9. J. B. Pendry, A. J. Holden, and W. J. Stewart, "Extremely low frequency plasmons in metallic mesostructures," Phys. Rev. Lett. **76**, 4773–4776 (1996).
10. J. B. Pendry, A. J. Holden, D. J. Robbins, and W. J. Stewart, "Low frequency plasmons in thin-wire structures," J. Phys. **10**, 4785–4809 (1998).
11. J. B. Pendry, A. J. Holden, D. J. Robbins, and W. J. Stewart, "Magnetism from conductors and enhanced nonlinear phenomena," IEEE Trans. Microwave Theory Tech. **47**, 2075–2084 (1999).
12. D. R. Smith, W. J. Padilla, D. C. Vier, S. C. Nemat-Nasser, and S. Schultz, "Composite medium with simultaneously negative permeability and permittivity," Phys. Rev. Lett. **84**, 4184–4187 (2000).
13. H. L. Luo, Z. Z. Ren, W. X. Shu, and S. C. Wen, "Reversed propagation dynamics of Laguerre-Gaussian beams in left-handed materials," Phys. Rev. A **77**, 023812 (2008).
14. H. C. Lin and J. X. Pu, "Propagation of Airy beams from right-handed material to left-handed material," Chin. Phys. B **21**, 054201 (2012).
15. B. Chen, C. D. Chen, X. Peng, and D. M. Deng, "Propagation of Airy Gaussian vortex beams through slabs of right-handed materials and left-handed materials," J. Opt. Soc. Am. B **32**, 173–178 (2015).
16. O. Livier and M. Soares, *Airy Functions and Applications to Physics* (ICP, 2004).
17. J. Zhou, H. Luo, and S. C. Wen, "ABCD matrix formalism for propagation of Gaussian beam through left-handed material slab system," Opt. Commun. **282**, 2670–2675 (2009).
18. A. E. Siegman, *Lasers* (University Science, 1986).
19. J. B. Pendry, "Negative refraction makes a perfect lens," Phys. Rev. Lett. **85**, 3966–3969 (2000).
20. J. D. Jackson, *Classical Electrodynamics* (Wiley, 1999).
21. H. L. Luo, S. C. Wen, W. X. Shu, and D. Y. Fan, "Role of transverse-momentum currents in the optical Magnus effect in free space," Phys. Rev. A **81**, 053826 (2010).
22. A. Y. Bekshaev and M. S. Soskin, "Transverse energy flows in vectorial fields of paraxial beams with singularities," Opt. Commun. **271**, 332–348 (2007).
23. Y. Harada and T. Asakura, "Radiation forces on a dielectric sphere in the Rayleigh scattering regime," Opt. Commun. **124**, 529–541 (1996).
24. J. A. Stratton, *Electromagnetic Theory* (McGraw-Hill, 1941).
25. M. Kerker, *The Scattering of Light and Other Electromagnetic Radiation* (Academic, 1969).